Braz J Phys (2015) 45:288–295
DOI 10.1007/s13538-015-0312-4

CONDENSED MATTER

Modeling of High-Quality Factor XNOR Gate Using Quantum-Dot Semiconductor Optical Amplifiers at 1 Tb/s

Amer Kotb

Received: 22 October 2014 / Published online: 17 March 2015

Abstract The modeling of all-optical logic XNOR gate is realized by a series combination of XOR and INVERT gates. This Boolean function is simulated by using Mach–Zehnder interferometers (MZIs) utilizing quantum-dots semiconductor optical amplifiers (QDs-SOAs). The study is carried out when the effect of amplified spontaneous emission (ASE) is included. The dependence of the output quality factor (*Q*-factor) on signals and QDs-SOAs' parameters is also investigated and discussed. The simulation is conducted under a repetition rate of ~1 Tb/s.

Keywords XNOR gate · 1 Tb/s · Quantum-dot semiconductor optical amplifier · Amplified spontaneous emission

1 Introduction

An important step in the development of all-optical logic technology, which includes key functionalities in fundamental and system-oriented level such as buffering, demultiplexing, clock recovery, packet processing, wavelength conversion, data regeneration, optical encryption/decryption etc., is the demonstration of optical logic elements that can operate at ultra high speeds. In recent years, demonstrations of high-speed all-optical logic gates using different schemes based on semiconductor optical amplifiers (SOAs) have been reported [1–10]. Among these approaches, SOA is believed to be a key component for all-optical logic gates, because it has a stronger nonlinearity than optical fibers and it can be integrated more easily. However, the speed of conventional bulk SOA operation is limited by the finite gain and phase recovery time of their temporal response.

For a quantum-dot (QD) SOA, the gain recovery response is significantly faster (i.e., 300 fs–10 ps) than for bulk and quantum-well (QW) SOA, which can lead to a considerably improved high-speed performance for QD-SOA-based logic systems. The QD-SOA high-bit-rate signal processing up to 160 Gb/s and a new scheme of 3R regenerators have been presented [11]. The main advantage of QD-SOAs, as compared to the bulk and QW-SOAs is based on the existence of the gap between the QD levels and wetting layer as well as on the lower cross section of carrier-photon interaction, which results, in particular, in shorter carrier relaxation times and lower gain saturation [12, 13]. The performances of all-optical logic and the high speed potential of QD-SOA-based devices have been studied [14–25]. A proposal for ultrafast all-optical XNOR gate using single QD-SOA-Mach–Zehnder interferometer (MZI) has been theoretically implemented at 250 Gb/s [26] up to 1 Tb/s [27]. 1 Tb/s high-quality factor NOR and NAND gates based on QD-SOAs with effect of amplified spontaneous emission (ASE) [28, 29] are discussed. In this work, we continue, extend, complete, and generalize the relevant previous work [28, 29] by investigating the high-speed performance of the other important QD-SOA-based all-optical logic XNOR gate with the help of numerical simulation conducted at a repetition rate of ~1 Tb/s. To investigate the "quality" of XNOR operation by simulation, the *Q*-factor of the XNOR output signal has been calculated. This metric gives information for the optical signal to noise ratio in digital communications and is defined as $Q=(S_1-S_0)/(\sigma_1+\sigma_2)$ [30], where S_1 and S_0 are the average intensities of the expected "1"s and "0"s and σ_1 and σ_2 are the standard deviations of those intensities. The impact on the quality factor (*Q*) of a

A. Kotb (✉)
Department of Physics, Faculty of Science, Fayoum University, Fayoum 63514, Egypt
e-mail: amer_22003@yahoo.com

A. Kotb
e-mail: kotb@phys.uconn.edu

number of parameters, including ASE, which depends on spontaneous emission factor (N_{sp}) of the amplifier [5–7], single pulse energy, injected current density, input pulse width, transition lifetime, linewidth enhancement factor (α-factor), and saturation power is investigated. The employed model supposes two discrete QD energy levels acting on carrier dynamics and takes into account the nonlinear effects. The derived results show that provided the critical parameters are suitably optimized, these gates can exhibit a Q-factor higher than that reported in ref. [27], where the effect of ASE was neglected and not modeled as suggested in [5–7].

2 QD-SOA-MZI Model

The operation of a QD-SOA can be studied using a rate-equation model as in refs. [14–26]. The transition between the wetting layer, the QD excited state, and the QD ground state is schematically illustrated in refs. [28, 29]. Carriers are injected into the wetting layer from which they make a fast transfer to the QDs. The device gain is determined by the carrier density of the QD ground state. Since the wetting layer serves as the only recipient of the pump current, while the QD excited state serves as a carrier reservoir for the ground state with ultra fast carrier relaxation to the latter, their carrier densities and transition rates can affect the device gain. The rate equation for carriers in wetting layer and a single QD is described in refs. [14, 15].

The device used is the commonly employed InAs/GaAs QD-SOA, with InAs QDs embedded in GaAs layer. The active layer of the device consists of alternately stacked InAs island layers and GaAs intermediate layers. A two-level QD model is used to simulate the carrier transitions in the QD-SOA device. The carrier heating results from a thermalization of carriers in the entire energy band following the pulse. This is a fast process occurring in a time scale of 0.1 to 0.7 ps. The injected pulse reduces the gain at the photon energy of this excitation, i.e., it burns a hole in the gain spectrum known as spectral hole burning (SHB). The schematic diagram of the QD-SOA-MZI for XNOR operation is shown in Fig. 1.

The exact model for QD-SOA and its solution are described in refs. [14, 15]. By taking into consideration both carrier heating (CH) and SHB effects, the time-dependent gain for each QD-SOA is given by [28, 29]:

$$\frac{dh_d}{dt} = \frac{h_w}{\tau_{d\to w}}\left(1-\frac{h_d}{h_0}\right) - \frac{h_d}{\tau_{dr}} - [\exp(h_d + h_{\mathrm{CH}} + h_{\mathrm{SHB}}) - 1]S(t,0)\,, \quad (1)$$

$$\frac{d\,h_w}{d\;t} = \frac{h_{in}}{\tau_{w\;\;r}}\left(1-\frac{h_w}{h_0}\right) - \frac{h_w}{\tau_{w\;\;r}} - \frac{h_w}{\tau_{w\to d}}\left(1-\frac{h_d}{h_0}\right)\,, \quad (2)$$

$$\frac{d\,h_{\mathrm{CH}}}{d\;t} = -\frac{h_{\mathrm{CH}}}{\tau_{\mathrm{CH}}} - \frac{\varepsilon_{\mathrm{CH}}}{\tau_{\mathrm{CH}}}[\exp(h_d + h_{\mathrm{SHB}} + h_{\mathrm{CH}}) - 1]S(t,0)\,, \quad (3)$$

$$\frac{dh_{\mathrm{SHB}}}{dt} = -\frac{h_{\mathrm{SHB}}}{\tau_{\mathrm{SHB}}} - \frac{\varepsilon_{\mathrm{SHB}}}{\tau_{\mathrm{SHB}}}[\exp(h_d + h_{\mathrm{SHB}} + h_{\mathrm{CH}}) - 1]S(t,0) - \frac{dh_d}{dt} - \frac{dh_{\mathrm{CH}}}{dt}\,, \quad (4)$$

$$h_{in} = \int_0^z \frac{a\,J\,\tau_{wr}}{e\,d}\,d\;z'. \quad (5)$$

The total gain is given by:

$$G(t,z) = \exp[h_{\mathrm{total}}(t)] = \exp[h_d(t) + h_{\mathrm{CH}}(t) + h_{\mathrm{SHB}}(t)]\,, \quad (6)$$

where $h(t)$ is an integral of optical gain per unit length over the length of QD-SOA and h_{total} equals the sum of h_d, h_{CH}, and h_{SHB}. $S(t, 0)$ is the instantaneous input optical intensity inside the QD-SOA and h_d, h_w, h_{CH}, and h_{SHB} are the h-factor values for carriers' recombination between the wetting layers and the QDs, carrier heating and spectral hole burning, respectively. h_0 is the maximum value of integrated gain and G_0=exp [h_0] is the unsaturated power gain. $\tau_{w\to d}$ is the transition rate between wetting layer and ground state in the quantum dot, τ_{wr} is

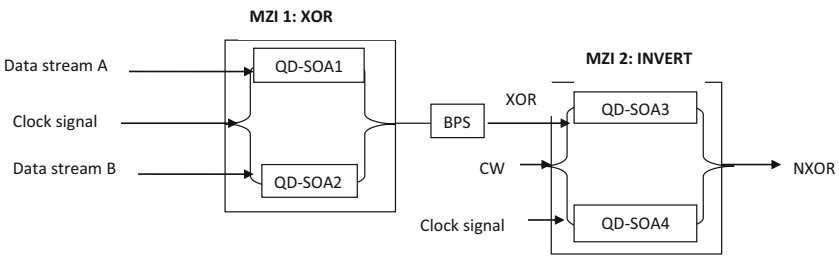

Fig. 1 Schematic of a XNOR logic gate using two MZIs in series combination. *BPF* band-pass filter

the carrier recombination rate in wetting layer, $\tau_{d\to w}$ is the excitation rate from ground state to wetting layer and τ_{dr} is the recombination rate in semiconductor dot. τ_{SHB} is the carrier-carrier scattering rate while τ_{CH} is the temperature relaxation rate. $\varepsilon_{\mathrm{SHB}}$ and $\varepsilon_{\mathrm{CH}}$ are the nonlinear gain suppression factors due to SHB and CH. a is the differential gain of QD-SOA (that is, $a=2\times10^{-15}$ cm^2), J is the injection current density, d is the total wetting layer thickness, and e is the electron charge. Factor α is derived from the density of states and Fermi function in the QD and wetting layer. It represents the ratio of carriers in the wetting layer and in QDs. Large number of carriers is present in the wetting layer which makes a fast transfer to QD when the QD carriers are depleted. The phase response is related to the temporal gain as:

$$\phi(t) = -0.5[\alpha\ h_d(t) + \alpha_{\mathrm{CH}} h_{\mathrm{CH}}(t)], \tag{7}$$

where α is the traditional linewidth enhancement factor, α_{CH} is the linewidth enhancement due to CH and α_{SHB} is the linewidth enhancement due to SHB. The contribution α_{SHB} is almost zero since SHB produces a nearly symmetrical spectral hole centered at the signal wavelength, so that the Kramers-Kronig integrand becomes antisymmetric around the operating frequency and the Kramers-Kronig integral remains small.

The data input to be Gaussian-shaped pulse streams is assumed to be:

$$P_{A,B}(t) = \sum_{n=-\infty}^{n=+\infty} a_{nA,B} \frac{2\sqrt{\ln(2)}P_0}{\sqrt{\pi}\tau_{\mathrm{FWHM}}} \mathrm{Exp}\left(-\frac{4\ln(2)(t-nT)^2}{\tau^2{}_{\mathrm{FWHM}}}\right), \tag{8}$$

where $a_{nA,B}$ represents the nth pulse in data streams A and B, which can take the logical value "1" or "0" with equal probability. Also, P_0 is the input pulse energy, T the bit period, and τ_{FWHM} the pulse width (full width at half maximum).

3 XNOR Model

3.1 Operation Principle

In this study, XNOR gate is realized by a series combination of XOR and INVERT gates as shown in refs. [5, 26]. For XOR operation, two data signals A and B are injected into the QD-SOAs incorporated in the upper and lower arms of MZI 1. A clock stream comprising of continuous "1"s is introduced in the setup from the middle input port of the configuration, as shown in Fig. 1. The data signals A and B, which are spectrally located at wavelengths λ_1 and λ_3, respectively, induce via cross-phase modulation (XPM) a phase shift in the split components of the clock signal, at wavelength λ_2, in each QD-SOA. Then the recombined clock signal at the output of MZI 1 carries the result of XOR operation between the binary content of data A and B. For proper signal discrimination wavelength λ_2 must be chosen so that it is different from λ_1 and λ_3, while λ_1 and λ_3 need not be different. Initially, MZI1 is balanced, and so when A="0" and B="0" the decomposed clock signal components traveling through the two MZI arms do not acquire any phase shift in the respective QD-SOAs. Thus, when they recombine at the output the result is "0." However, when A="1" and B="0," the clock signal replica traveling through the upper arm together with signal A acquires due to XPM a phase change, while its counterpart traveling through the lower arm does not suffer any such change. This results in "1" at the output. The same happens when A="0," B="1." However, when A="1" and B="1," the phase changes induced on the clock signal constituents traveling through both MZI arms are equal; hence, the output is "0." The INVERT operation is obtained similarly to XOR operation if one of the data inputs is replaced by a clock signal. Then in order to realize the XNOR operation, the XOR output from MZI1 is launched into the upper arm of MZI2. Concurrently, a continuous wave (CW) beam and another clock signal are launched into the middle and bottom input ports, respectively, as shown in Fig. 1. The effect of ASE on the performance of the XNOR gate is due to the contribution both from the XOR and INVERT operations.

The detuning between the signals must be less than the homogeneous broadening of the QD-SOAs so that switching can efficiently occur through XPM [31]. Since the homogeneous broadening, which is about 15 meV at room temperature, is smaller than the inhomogeneous broadening, which reaches 40 meV [11], this condition will also hold with respect to the inhomogeneous broadening that manifests in real QD-SOA devices due to fluctuations in the QDs size, shape, and composition. This means that this effect does not affect the outcome of our theoretical study on the all-optical XNOR Boolean logic for optical time division multiplexing (TDM) single channel at ultrafast data rate [32]. Therefore, no special consideration like dividing the QDs ensemble into different groups with energies depending on their resonant frequencies [11], while assuming a Gaussian-like distribution for the respective gain spectral profiles [33] is required to be made in our model.

3.2 Simulation

The employed numerical model has been formulated in such way so as to describe the main dynamic effects that occur inside the SOAs. The fundamental framework for doing this relies on a microscopic view of the amplification and propagation of optical pulses through a SOA as well as of the change of its carriers due to the interaction of the latter

with light. However, in the effort to maintain, for practical reasons, a good balance between mathematics and computer power, the physical processes that manifest inside a SOA subject to an intense optical signal have been considered in a phenomenological manner [34]. The adoption of this approach has been validated through extensive comparison between theory and experiment, which has revealed an excellent matching. Thus, the adopted model, which will use real SOAs' parameter values can produce accurate and realistic results and is mostly suitable for the purposes of the proposed project.

The main factors that need to be considered for the experimental demonstration of the scheme are primarily those that concern the practical availability of the data signals and SOAs. More specifically, the data signals must have the appropriate intensity level, pulse width, and format at an excessively high data rate. This means that they should be generated by laser systems and boosted by erbium-doped fiber amplifiers before being launched into the all-optical gates, which lies well within the capabilities of the relevant state-of-the-art technology [35, 36]. Similarly, the SOAs must have characteristics in terms of small signal gain, carrier lifetime, alpha factor, and saturation power that can be supported by such off-the-shelf devices, which is also feasible. Thus, in principle, it would be possible to construct laboratory prototypes of the proposed all-optical gates.

The modulated clock signal, which plays the role of the probe, interferes from the two arms of the MZIs obeying the following formula:

$$P_{\text{out}}(t) = 0.25\ P_C\left\{G_1(t) + G_2(t) - 2\sqrt{G_1(t)G_2(t)}\ \text{Cos}[\Phi_1(t) - \Phi_2(t)]\right\}, \tag{9}$$

where P_C corresponds to the input power of the CW probe signal entering the MZI configuration through the common port. $G_1(t)$ and $G_2(t)$ are the gain experienced by the control beam in each arm of QD-SOA-MZI and $\Phi_1(t) - \Phi_2(t)$ is the phase difference of the probe signal in the two arms.

The instantaneous optical intensity inside QD-SOA1 for the XOR gate is given by:

$$P_1(t) = P_A(t) + P_C\,, \tag{10}$$

$$P_2(t) = P_C + P_B(t)\,. \tag{11}$$

The instantaneous optical intensity inside QD-SOA2 for the XNOR gate is given by:

$$P_3(t) = P_{\text{XOR}}(t) + P_{\text{CW}}\,, \tag{12}$$

$$P_4(t) = P_{\text{CW}} + P_C\,. \tag{13}$$

The QD-SOA parameters' values are defined and taken throughout the simulation as listed in Table 1.

At 1 Tb/s, Fig. 2a illustrates the simulation results for the XNOR operation between an indicative pattern of data signal *A* and an indicative pattern of data signal *B* shown in the top two traces. The third trace shows for logical comparison the XOR output and the bottom trace shows the XNOR output after QD-SOA-MZIs 1 and 2, respectively. The eye diagram that corresponds to XNOR operation is shown in Fig. 2b. In the absence of ASE noise, the primary source of noise in the calculations, which lowers the *Q*-factor, is due to the pattern effects that result from long recovery times of gain and gain-induced phase changes. For an ideal amplifier (N_{sp}=2), the system's output *Q*-factor is 31 at 1 Tb/s.

The *Q*-factor relates to conventional digital circuit figures of merit, such as fan-in, fan-out, energy efficiency, latency, etc. Its desired value is the same as that for ensuring error-free performance for the all-optical gates, i.e., over six, which corresponds to a bit error rate of less than 10^{-9} [37]. However, whether this necessary condition will be satisfied cannot be known in advance and we will have to conduct an investigation, which will depend on the particular figure of merit. Thus, for fan-in and fan-out capability we will have to consider whether the proposed all-optical gates can handle more than two inputs or drive from their output port the input that controls switching of subsequent gates, respectively. Thus, in this case, the impact of the *Q*-factor will be revealed after applying and running the model for the composite configuration, and the result may differ from that obtained for a single gate.

Table 1 The QD-SOA parameters' values are defined and taken throughout the simulation

Symbol	Definition	Value
P_0	Input pulse energy	0.2 pJ
τ_{FWHM}	Pulse width	0.4 ps
$\tau_{w\to d}$	Transition rate between wetting layer and ground state	5 ps
$\tau_{d\to w}$	Excitation rate from ground state to wetting layer	10,000 ps
τ_{wr}	Carrier recombination rate in wetting layer	2200 ps
τ_{dr}	Recombination rate	400 ps
τ_{CH}	Temperature relaxation rate	0.3 ps
τ_{SHB}	Carrier–carrier scattering rate	0.1 ps
$\varepsilon_{\text{CH}}=\varepsilon_{\text{SHB}}$	Nonlinear gain suppression factors	0.08 W^{-1}
α	Differential gain	2×10^{-15} cm^2
J	Injection current density	4 kA/cm^2
d	Wetting layer thickness	0.5 μm
α	Traditional linewidth enhancement factor	5
α_{CH}	Carrier-heating alpha factor	1
α_{SHB}	Spectral hole-burning alpha factor	0
P_{sat}	Saturation power	20 mW

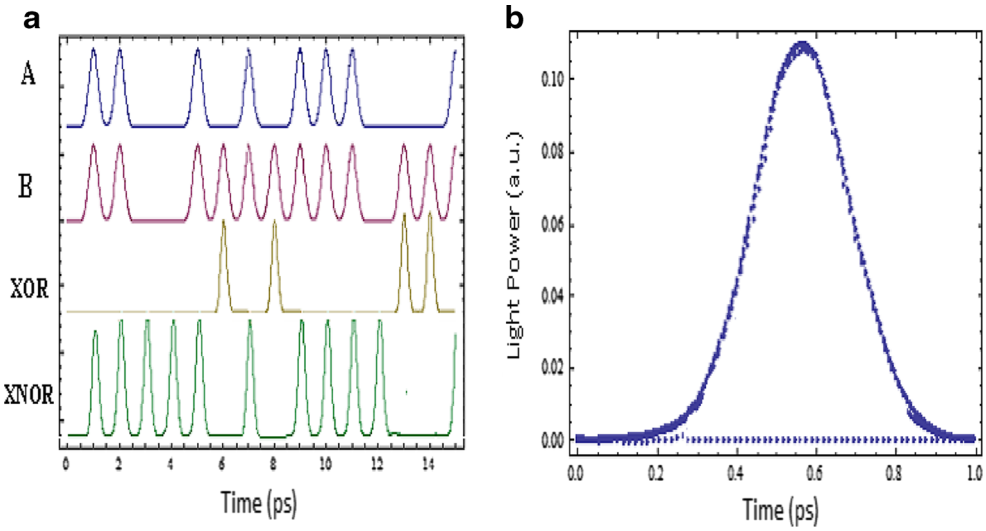

Fig. 2 The simulation results of QD-SOA-MZI for XNOR operation. **a** Top two traces are the signals *A* and *B*; the third trace is the XOR output shown for logical comparison and the bottom trace is XNOR output. **b** The eye diagram for XNOR gate

Nevertheless, reports on this issue from other studies that have exploited technologically advanced SOAs in combination with the advantages of the MZI [24] make us feel that it should be possible to attain at least the minimum requirement for the *Q*-factor. This means that the *Q*-factor may not be so significant for this figure of merit, much more when all signals involved in switching travel in the same direction [38]. Finally, since the energy efficiency is determined by the peak data power, SOAs bias current, and switched output power [24], selecting the two first parameters so that the standards set for the *Q*-factor are met at the gate's exit will also be favorable for the specific figure of merit.

The ASE causes additional output noise through spontaneous–spontaneous beat noise and signal–spontaneous beat noise. In addition, if one were to measure the bit error rate at the gate output, the dark current of the photodiode, shot noise, and thermal noise should also have to be considered. An analysis of all these noise terms is given in Chapter 6 of ref. [30] when the QD-SOA is used as a pre-amplifier. The ASE-related noise depends on N_{sp} of the amplifier according to the relation [5–7]:

$$P_{ASE} = N_{sp}(G-1)h\ \upsilon B_0\ , \tag{14}$$

where G is the maximum gain, h is Plank's constant, υ is the light frequency, and B_0 is the bandwidth.

The ASE noise calculated using Eq. (14) is added numerically to the pattern effect noise to obtain the *Q*-factor within the input pulse trains. The effect of ASE can be experimentally verified by connecting a wideband (few nm wide) optical unmodulated signal to the data input and measuring the *Q*-

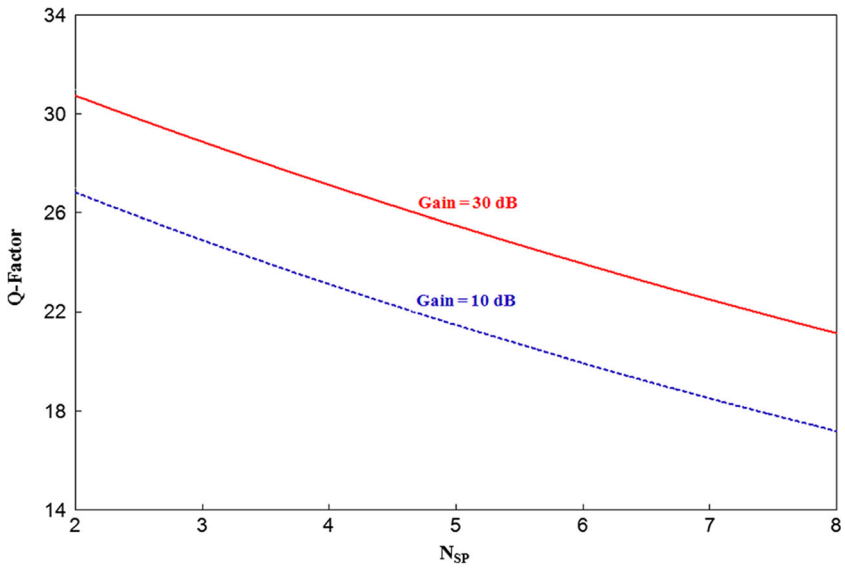

Fig. 3 *Q*-factor versus N_{sp} for XNOR operation at 1 Tb/s

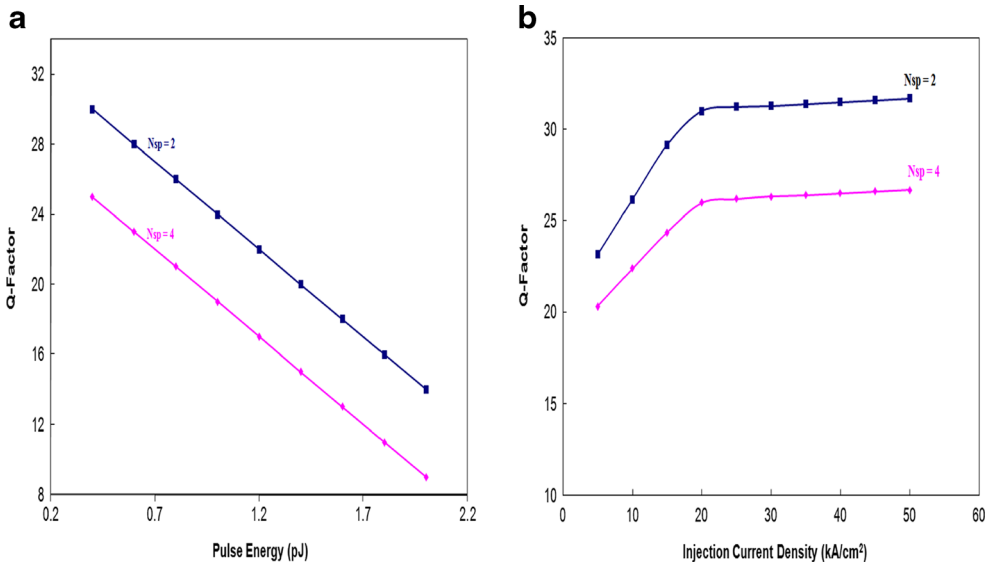

Fig. 4 *Q*-factor versus **a** input pulse energy and **b** injection current density for XNOR operation at 1 Tb/s

factor as a function of the intensity and bandwidth of this signal. Finally, ASE effects are important and must be taken into account when all-optical logic gates are cascaded to form more complex circuits and subsystems of enhanced functionality. The *Q*-factor versus N_{sp} for the XNOR output at gains of 10 and 30 dB is shown in Fig. 3.

At 1 Tb/s, the *Q*-factor versus input single pulse energies and injection current densities for different N_{sp} values has been calculated and shown in Fig. 4. An increase of the input pulse energy will saturate the QD-SOAs more easily, which results in a decrease in the *Q*-factor, as shown in Fig. 4a. Figure 4b illustrates the dependence of the *Q*-factor on the injection current. When the injection current to the wetting layer is increased, the performance of the XNOR gate improves, as shown by the increase in *Q*-factor. This can be understood by the fact that with this change more carriers are available to compensate for the carriers depleted in the active QDs. With an increase in the injection current, the maximum achievable *Q*-factor increases linearly with this parameter. This result is consistent with the saturation effect of QD-SOA.

For XNOR operation, the *Q*-factor versus pulse width, and transition lifetime at different N_{sp} values is shown in Fig. 5. The *Q*-factor decreases when increasing the pulse width because two neighboring pulses tend to overlap for wider pulse width as shown in Fig. 5a. Figure 5b shows the dependence of *Q*-factor on the transition lifetime. The results show that the *Q*-factor decreases as the transition lifetime increases. The transition lifetime determines the speed of gain and phase recovery in the active region, so the *Q*-factor is higher for a shorter transition time.

The linewidth enhancement factor (α-factor) depends on the relative position of the amplifier gain peak and the signal wavelengths and thus can vary. The *Q*-factor as a function of

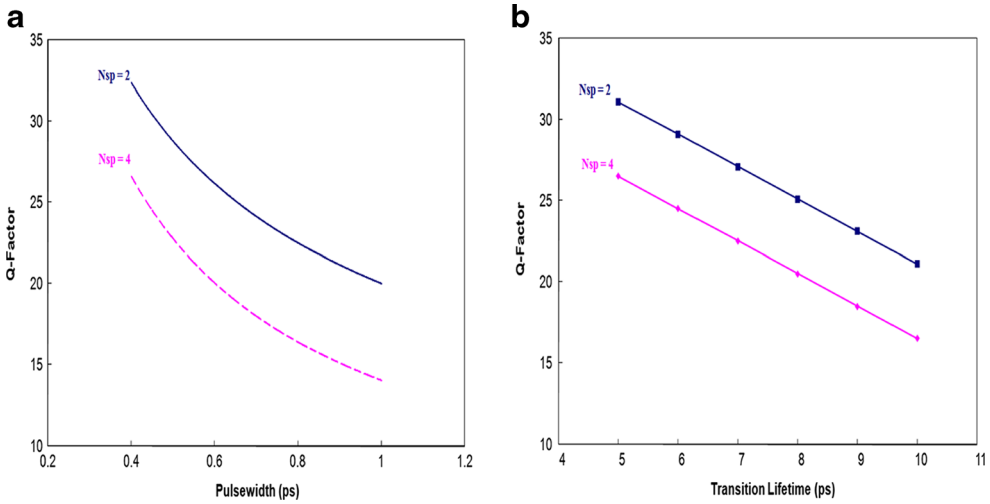

Fig. 5 **a** Calculated *Q*-factor as a function of pulse width. **b** Dependence of calculated *Q*-factor on transition lifetime for XNOR operation

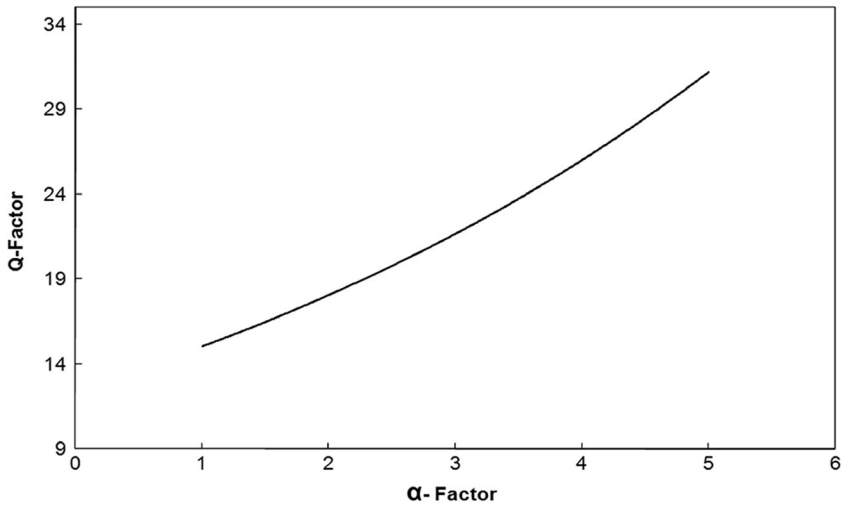

Fig. 6 The simulated Q-factor dependence on linewidth enhancement factor (α-factor) for XNOR operation

α-factor at 1 Tb/s is shown in Fig. 6. The Q-factor is larger for larger α-factor because the phase changes are larger for large α-factor and, hence, the XNOR signal ("1" values) is larger. This increases the signal to noise ratio and, hence, the Q-value.

Note that the gain of the SOA saturates when the optical power is comparable to the saturation power (P_{sat}) [39, 40]. The saturation power dependence of the QD-SOA-MZI output has been calculated at two different N_{sp} values as shown in Fig. 7. From Fig. 7, it is seen clearly that Q-factor increases with increasing P_{sat}.

4 Conclusion

In conclusion, the performance of an all-optical logic XNOR gate based on quantum dot-semiconductor optical amplifiers (QD-SOAs) has been simulated. The impact on the quality factor (Q) of a number of parameters, including amplified spontaneous emission (ASE), which depends on spontaneous emission factor (N_{sp}) of the amplifier, single-pulse energy, injected current density, input pulse width, transition lifetime, linewidth enhancement factor (α-factor), and saturation power is investigated. The simulation is conducted under a repetition rate of ~1 Tb/s. The achieved quality factor (Q-factor) was 31 for low-input pulse power. A decrease in the Q-factor is predicted for high spontaneous emission factor (N_{sp}). An increase of input pulse energy will saturate the QD-SOAs more easily, which results in a decrease in the Q-factor. When the injection current to the wetting layer is increased, the performance of the XNOR gate improves. The Q-factor decreases when increasing the pulse width. The Q-factor is higher for shorter transition time. The Q-factor is larger for larger α-factor and saturation power.

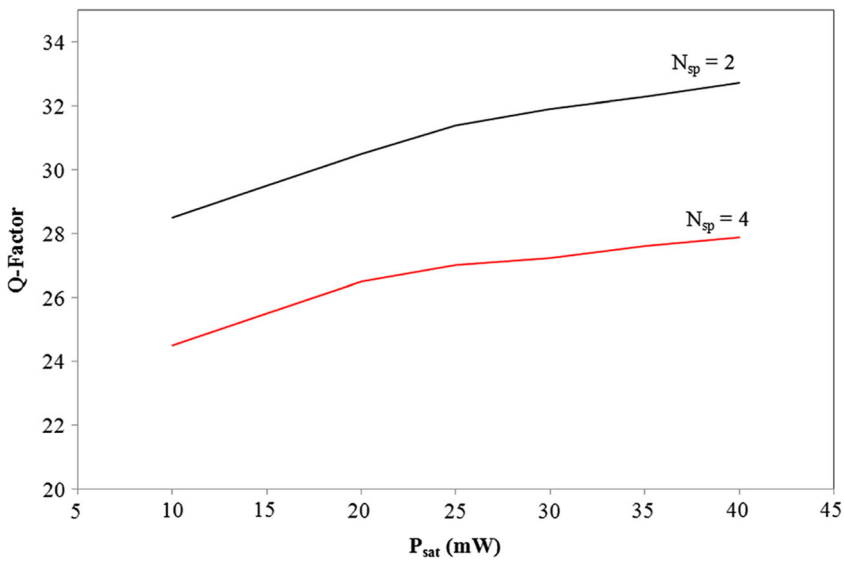

Fig. 7 Calculated Q-factor as a function of saturation power (P_{sat}) at two different N_{sp} values for XNOR operation

Acknowledgments The authors would like to thank the editors of the journal and anonymous referees for the important comments that helped me to improve the content of this paper.

References

1. K.E. Zoiros, G. Papadopoulos, T. Houbavlis, G.T. Kanellos, Opt. Commun. **258**, 114 (2006)
2. C. Bintjas, M. Kalyvas, G. Theophilopoulos, T. Stathopoulos, H. Avramopoulous, L. Occhi, L. Schares, G. Guekos, S. Hansmann, R. Dall'Ara, IEEE Photon. Technol. Lett. **12**, 834 (2000)
3. T. Fjelde, D. Wolfson, A. Kloch, B. Dagens, A. Coquelin, I. Guillemot, F. Gaborit, M. Renaud, Electron. Lett. **36**, 1863 (2000)
4. H. Chen, G. Zhu, J. Jaques, J. Leuthold, A.B.. Piccirilliand, N.K. Dutta, Electron. Lett. **38**, 1271 (2002)
5. A. Kotb, J. Maeda, Optoelectron. Lett. **8**, 437 (2012)
6. A. Kotb, S. Ma, Z. Chen, N.K. Dutta, G. Said, Opt. Commun. **284**, 5798 (2011)
7. A. Kotb, *All-optical logic gates using semiconductor optical amplifier*, 1st edn. (LAMBERT Academic Publishing, Germany, 2012)
8. H. Dong, H. Sun, Q. Wang, N.K. Dutta, J. Jaques, Microw. Opt. Technol. Lett. **48**, 1672 (2006)
9. H. Sun, Z. Chen, S. Ma, N.K. Dutta, Proc. SPIE **6775**, 67750 (2007)
10. Q. Wang, H. Dong, H. Sun, N.K. Dutta, Opt. Commun. **260**, 81 (2006)
11. M. Sugawara, T. Akiyama, N. Hatori, Y. Nakata, H. Ebe, H. Ishikawa, Meas. Sci. Technol. **13**, 1683 (2002)
12. A.V. Uskov, T.W. Berg, J. Mørk, IEEE J. Quant. Electron. **40**, 306 (2004)
13. Y. Ben-Ezra, M. Haridim, B.I. Lembrikov, IEEE Photon. Technol. Lett. **17**, 1803 (2005)
14. H. Sun, Q. Wang, H. Dong, N.K. Dutta, Microw. Opt. Technol. Lett. **48**, 29 (2006)
15. S. Ma, Z. Chen, H. Sun, N.K. Dutta, Opt. Express **18**, 6417 (2010)
16. A. Kotb, Opt. Quant. Electron. **45**, 473 (2013)
17. A. Kotb, Optoelectron. Lett. **9**, 89 (2013)
18. A. Kotb, K.E. Zoiros, Opt. Quant. Electron. **46**, 977 (2014)
19. E. Dimitriadou, K.E. Zoiros, Prog. Electromagn. Res. B (PIERS) **50**, 113 (2013)
20. Z.V. Rizou, K.E. Zoiros, A. Hatziefremidis, M.J. Connelly, J. Sel. Top. Quant. Electron. **19**, 1 (2013)
21. E. Dimitriadou, K.E. Zoiros, Optics **14**, 105401 (2012)
22. E. Dimitriadou, K.E. Zoiros, Opt. Laser Technol. **44**, 600 (2012)
23. E. Dimitriadou, K.E. Zoiros, Opt. Commun. **285**, 1710 (2012)
24. E. Dimitriadou, K.E. Zoiros, Opt. Laser Technol. **44**, 1971 (2012)
25. E. Dimitriadou, K.E. Zoiros, Opt. Laser Technol. **45**, 79 (2013)
26. A. Kotb, K.E. Zoiros, Opt. Quant. Electron. **45**, 1213 (2013)
27. A. Rostami, H. Nejad, R. Qartavol, H. Saghai, IEEE J. Quant. Electron. **46**, 354 (2010)
28. A. Kotb, Opt. Quant. Electron. **45**, 1258 (2013)
29. A. Kotb, K.E. Zoiros, Comput. Electron. **13**, 555 (2014)
30. N.K. Dutta, Q. Wang, *Semiconductor optical amplifiers*, 2nd edn. (World Scientific, New York, 2006)
31. Y. Ben-Ezra, M. Haridim, B.I. Lembrikov, M. Ran, IEEE Photon. Technol. Lett. **20**, 484 (2008)
32. A. Bogoni, L. Potì, P. Ghelfi, M. Scaffardi, C. Porzi, F. Ponzini, G. Meloni, G. Berrettini, A. Malacarne, G. Prati, Opt. Fiber Technol. **13**, 1 (2007)
33. Y. Ben-Ezra, B.I. Lembrikov, M. Haridim, IEEE Quant. Electron. **43**, 730 (2007)
34. G. Toptchiyski, S. Kindt, K. Petermann, E. Hilliger, S. Diez, H.G. Weber, Lightwave Technol. **17**, 2577 (1999)
35. H.C.H. Mulvad, M. Galili, L.K. Oxenløwe, H. Hu, A.T. Clausen, J.B. Jensen, C. Peucheret, P. Jeppesen, Opt. Express **18**, 1438 (2010)
36. D.R. Zimmerman, L.H. Spiekman, Lightwave Technol. **22**, 63 (2004)
37. G.P. Agrawal, *Fiber-optic communication systems*, 3rd edn. (Wiley, New York, 2002)
38. S. Bischoff, A. Buxens, S.T. Fischer, M. Dülk, A.T. Clausen, H.N. Poulsen, J. Mørk, Opt. Quant. Electron. **33**, 907 (2001)
39. Q. Wang, G. Zhu, H. Chen, J. Jaques, J. Leuthold, B. Piccirilli, N.K. Dutta, IEEE J. Quant. Electron. **40**, 703 (2004)
40. H. Dong, Q. Wang, G. Zhu, J. Jaques, A.B.. Piccirilli, N.K. Dutta, Opt. Commun. **242**, 479 (2004)